

High Peak Power RF Processing Studies of 3 GHz Niobium Cavities*

J. Graber, P. Barnes, J. Kirchgessner, D. Moffat, H. Padamsee, D. Rubin, and J. Sears
Laboratory of Nuclear Studies, Cornell University
Ithaca, New York 14853

Abstract

Field emission is the primary obstacle to improving accelerating gradients in superconducting RF cavities. We are investigating High Peak Power (HPP) Pulsed RF Processing as a means of reducing field emission loading in 3 GHz niobium accelerator cavities. Our apparatus includes a 3 GHz Klystron capable of delivering RF pulses of up to 200 kW peak power with pulse length up to 2.5 msec at a repetition rate of approximately 1 Hz. The input coupler has variable coupling such that the input external Q varies between 10^5 and 10^{10} without breaking the cavity vacuum. Low power, continuous wave (cw) tests before and after HPP show that HPP is effective in removing emissions which are unaffected by low power RF processing. CW measurements show that field emission reduction is dependent on maximum field reached during HPP. During processing, single cell cavities have reached pulsed fields of $E_{\text{peak}} = 70\text{--}72$ MV/m. These tests showed FE elimination to $E_{\text{peak}} = 40$ MV/m, and maximum fields of $E_{\text{peak}} = 50\text{--}55$ MV/m. Temperature mapping is used to characterize emissions before and after HPP Processing. Several cavities have been examined in a Scanning Electron Microscope following RF cold tests. The HPP technique is also being investigated in a nine cell cavity in order to prove applicability to multi-cell structures. The nine cell cavity has been successfully tested three times and through HPP has had achievable gradients increased from $E_{\text{acc}} = 10\text{--}14$ MV/m to $E_{\text{acc}} = 16\text{--}20$ MV/m.

I. EXPERIMENTAL APPARATUS

This project, its associated hardware, and early results were previously described in papers presented at the 4th Workshop on RF Superconductivity[1], and the 1989 and 1991 Particle Accelerator Conferences[2,3]. This paper will concentrate largely on progress made since those reports.

HPP Test Stand and Klystron

A diagram of the HPP test stand is shown in Figure 1. The high power klystron circuit diagram may be found in reference [1].

The HPP test stand was specially designed and constructed for the studies described here. The input RF coupling was designed to provide Q_{ext} between 10^5 (for HPP Processing) and 10^{10} (for low power cw tests) without breaking the cavity vacuum, thus avoiding surface contamination and associated emission between processing and subsequent cw low power testing. The coupling variation is provided through a variable

length outer conductor in the coaxial probe region. The cavity is moved up and down with respect to the fixed position input probe. The RF circuit of the test stand is designed to transmit over a 100 MHz wide band, centered on 3 GHz. Static heat leaks are estimated at ≤ 5 W. The test stand has two separate vacuum systems: 1) the UHV vacuum for the cavity interior, and 2) the waveguide vacuum which prevents air from condensing in the portion of the waveguide which is inside the dewar. These vacuums are separated by a coaxial window located below the cavity position. In order to minimize contaminants dropping into the cavity from above, only the top plane with a transmitted power probe is situated above the cavity.

Cavity Temperature Mapping System

A recent addition to the HPP test apparatus is a 100 thermometer temperature mapping system. This system is similar to the temperature mapping system which provided significant results in the 1.5 GHz program [4]. It consists of ten boards of ten thermometers each, spaced at 36° intervals around the azimuth of the cavity.

A temperature map (see Figure 6) consists of a ten by ten array of the differences of the outer wall temperature between RF on and RF Off. Each position on the map corresponds to an individual thermometer. Calibration of the thermometers is done via a calibrated germanium resistance thermometer.

A map can be obtained in approximately 25 seconds when the cavity is operated cw. Temperature maps may also be obtained during HPP pulsing. HPP maps are obtained in about 120 seconds, as the resistors are read one resistor per RF pulse. Temperature maps were instrumental in detection of the GTI phenomenon (see section II below). Additionally, HPP temperature maps allow distinction between the various types of breakdown events encountered either cw or during the pulsed high power processing.

II. EXPERIMENTAL RESULTS

Procedure

The experimental procedure is generally as follows, with minor alterations on individual tests:

1) One hour soak in HNO_3 , to remove metal contaminants, such as In or Cu. (See discussion of SEM examination below.)

2) Light (2-4 minutes) chemical etch in 1:1:2 (HNO_3 :HF: H_3PO_4) BCP, followed by extensive rinsing and mounting to test stand in clean room environment. (NOTE: Cavities initially had 100 microns removed from their surface via 1:1:1 BCP, prior to equator weld. In light of recent results on

* Supported by N.S.F. with supplementary support from the U.S.-Japan Collaboration.

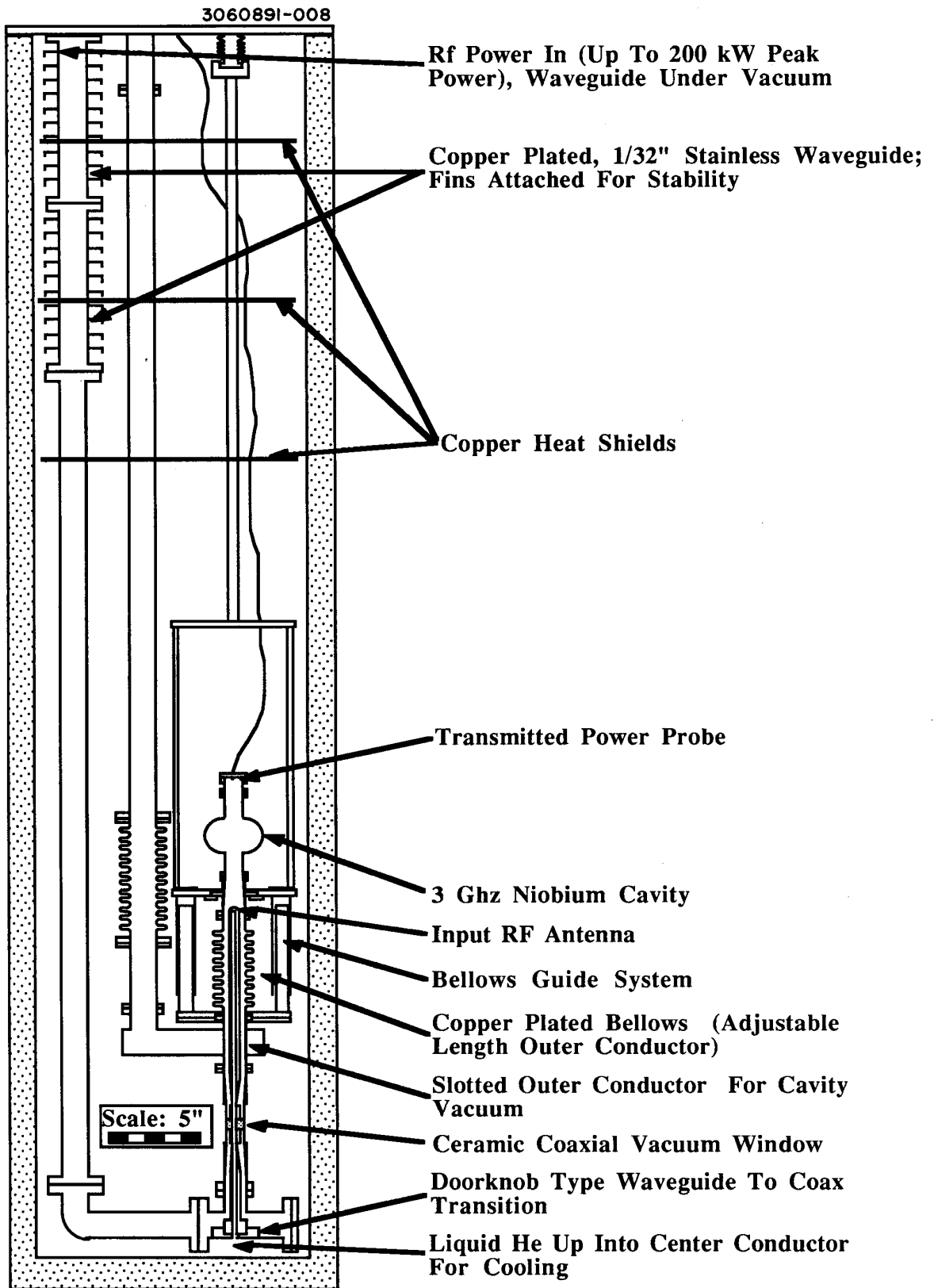


Figure 1. The HPP Experimental Test Apparatus in detail.

hydrogen contamination [5], all subsequent etchings are done for short periods with 1:1:2 BCP as opposed to 1:1:1 BCP.)

3) Pre-cool 12-20 hours with liquid nitrogen. Transfer liquid helium, then lower the bath temperature to 1.4-1.5 K.

4) Low power (≤ 20 W) characterization of cavity: obtain a Q vs. E curve, and temperature maps (to count and characterize emitters) at various field levels. Calibrate the transmitted power probe

5) Pulsed HPP processing at a fixed input power level for 10-60 minutes monitoring field levels in the cavity via transmitted power. Figure 2a shows a multiple exposure picture of several transmitted power pulses on the oscilloscope, all with the same input power level. As can be seen, when the input coupling is increased, the transmitted power increases, and the decay time decreases. At a certain threshold value (dependent on the emission characteristics of the particular cavity under study), the transmitted power signal begins to show erratic events, thought to be a field breakdown, probably associated with a burst of FE activity. The pulse with the highest transmitted power in Figure 2a shows one of the erratic breakdown type events. Figure 2b is another example of a non-reproducible breakdown shape seen during the erratic behaviors.

After some time, these breakdowns will subside, and the pulse will have a generally reproducible shape. This reproducible shape can be either a "normal" fill and decay, or if the fields are high enough, it can be of a shape which we associate with repetitive thermal breakdown. Figure 2c (also the lower curves of Figure 2a) shows an example of a "normal" fill and decay. Figure 2d shows a reproducible breakdown type transmitted power pulse. We associate this transmitted power pulse with the GTI phenomenon (described below). The transmitted power is then increased, either by increasing input power or input coupling, and the cycle repeats. Usually we find that as the power and field levels increase, the time required until the erratic behavior stops also increases. We believe the settling of the pulse to a reproducible shape coincides with maximal RF processing at this field level.

5) Steps 3 and 4 are generally repeated until low power cw tests show no further reduction in field emission loading.

Overall Effect: Reduced Loading of Single Cell Cavities

HPP Processing has been found to be effective in raising FE thresholds (as determined by first x-ray detection) 60-80% above the initial levels reached in chemically polished cavities. Figure 3 shows a typical Q vs. E_{peak} plot before and after HPP processing.

HPP processing of single cell cavities has been shown to increase the FE threshold up to $E_{peak} = 40$ MV/m, and maximum attainable fields up to $E_{peak} = 50-55$ MV/m. Figure 4 shows the increase in FE threshold due to HPP Processing. It is interesting to note that the benefits of HPP processing appear to be related to the electric field level reached during the HPP stage, and not merely the processing power level. Figure 5 shows the relationships between maximum field reached during HPP and subsequent FE threshold and maximum attainable electric field for single cell cavities tested to date.

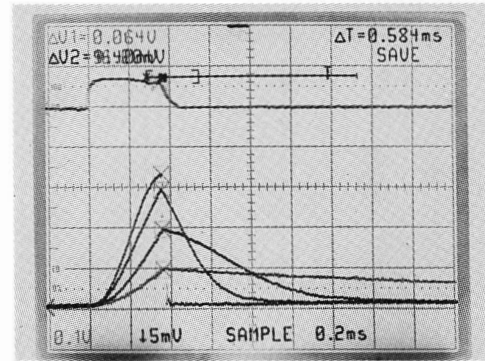


Figure 2a. Multiple exposure showing change in transmitted power with change in coupling.

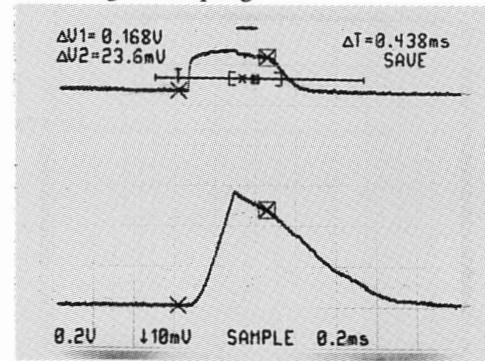


Figure 2b. Example of erratic, non-repeatable transmitted power pulse seen during HPP Processing.

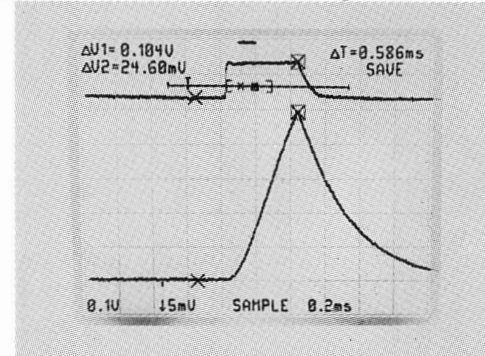


Figure 2c. Example of a transmitted power trace showing a "normal" fill and decay.

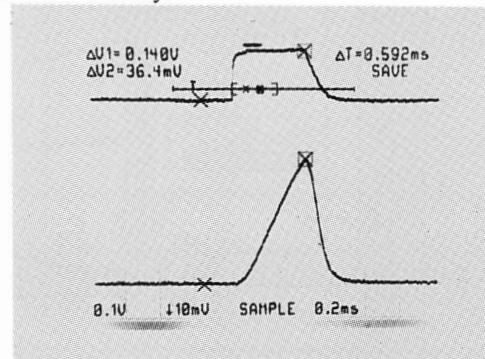


Figure 2d. Example a reproducible breakdown type event, which we believe to be associated with GTI.

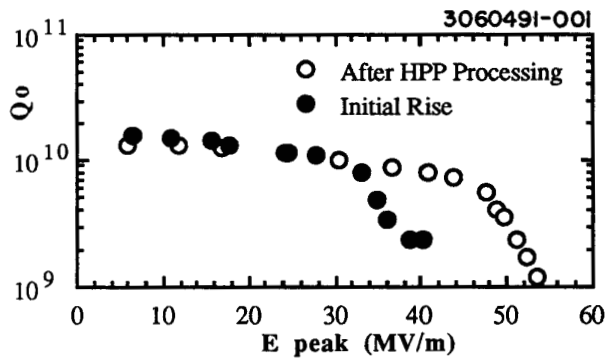


Figure 3. An example of the effect of HPP.

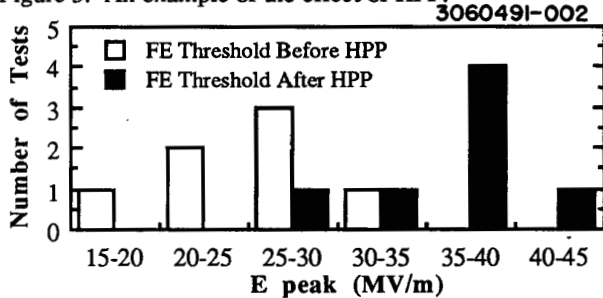


Figure 4. Comparison of the FE Threshold field with and without HPP Processing in 7 single cell cavity tests.

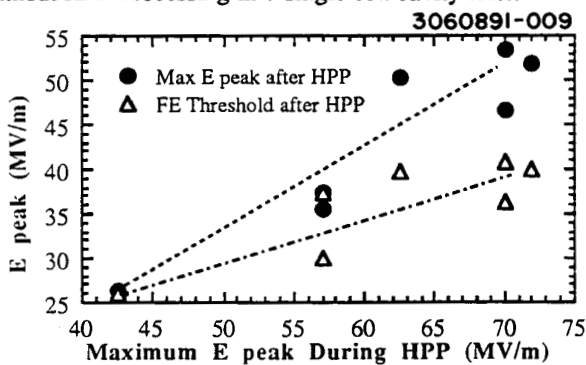


Figure 5. Maximum attainable cw electric field and FE Threshold Field as a function of maximum HPP field.

We have found the limit on maximum pulsed field during HPP to be 70-72 MV/m ($H_{peak} = 1670$ Oe). These field values were sustained for 2-5 μsec , followed by a rapid decay of the cavity fields. The limiting effect has been determined to be thermal breakdown, caused by the very high (≥ 1250 Oe) surface magnetic field. Decay times are less than 10 μsec , as would be expected for normal conducting niobium. Figure 6 shows a temperature map taken during HPP Processing, where this type of breakdown (transmitted power pulse shape shown in Figure 2d) was occurring.

We have labeled this effect Global Thermal Instability (GTI). In GTI, the high magnetic fields in the equator region cause power dissipation at such a rate that the entire equator region heats unstably until T_c is surpassed and a breakdown occurs. More details on this effect at cw fields are presented in another paper [6].

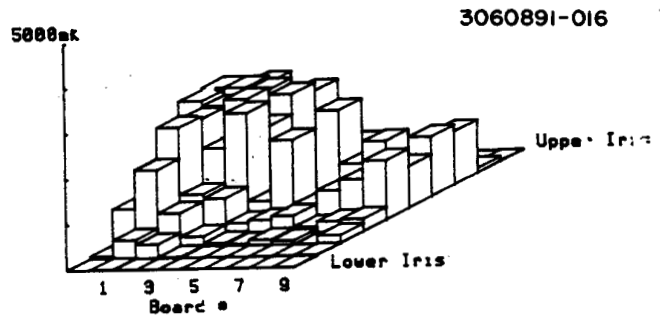


Figure 6. Temperature map taken during HPP Processing, with a transmitted power shape as shown in Figure 2d. The high temperature throughout the equator region of the cavity is characteristic of the Global Thermal Instability phenomenon.

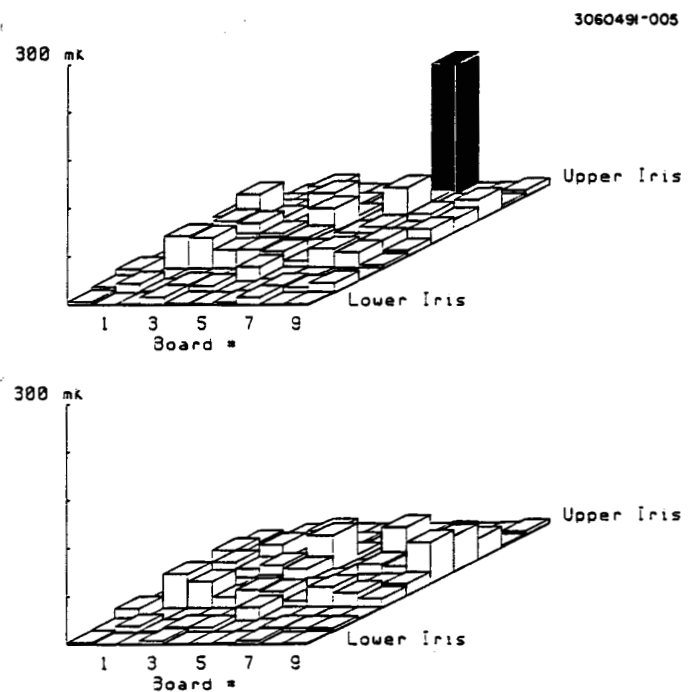


Figure 7. Temperature maps showing the removal of a strong field emission site with HPP Processing. The top map was taken at $E_{peak} = 48$ MV/m prior to HPP. The bottom map was taken at $E_{peak} = 49$ MV/m after HPP.

Local Effect:

Changed ΔT vs E Behavior From Temperature Maps

Addition of the temperature mapping system has allowed for a better determination of the local effects of HPP. Temperature maps are made before and after HPP processing. Figure 7 shows an example of the removal of a significant emitter. Often it appears that the effect of HPP is a decrease of emission, as opposed to complete destruction of the emitter. Figure 8 shows the evolution of a ΔT vs E_{peak} behavior of an emitter over the course of several HPP sessions as well as a room temperature cycle.

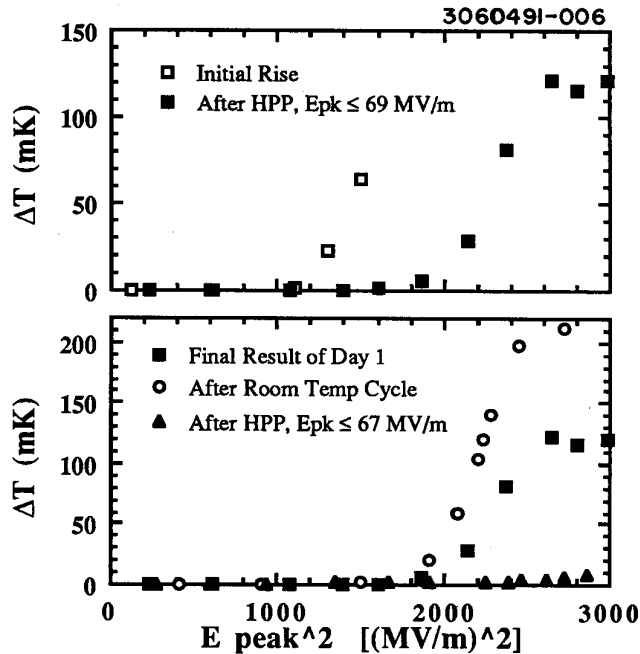


Figure 8. Evolution of ΔT vs E_{peak} squared over the course of several HPP sessions.

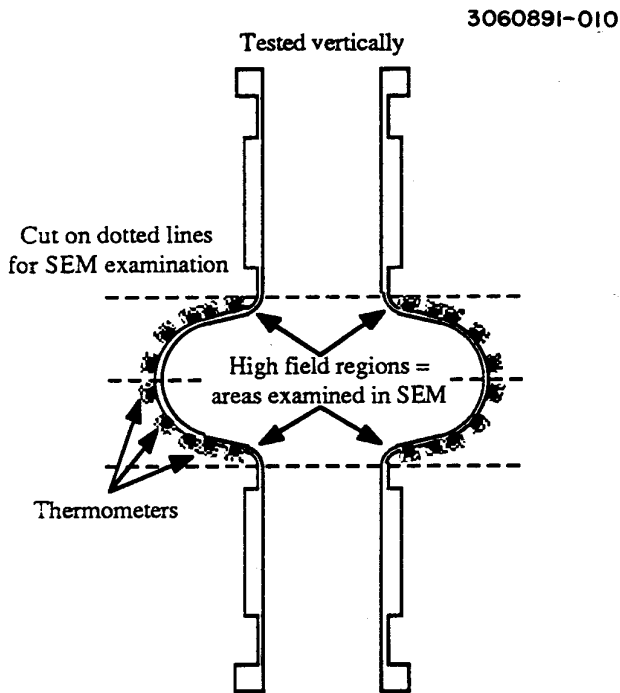


Figure 9. Diagram showing the area of cavity which was examined in the SEM, along with the location of the thermometers for temperature mapping (Drawing from D. Moffat).

Microscopic Effect:
SEM Investigations of Emission Sites

In an ongoing research effort with the "mushroom cavity" [7], Scanning Electron Microscope (SEM) examination of RF surfaces reveals significant surface features in areas which are

subject to field emission. Motivated by these findings, three 3 GHz cavities have been cut open following RF cold tests.

Figure 9 shows a diagram of a single cell S-band cavity with thermometer positions, as well as the dissection geometry used to examine the cavity in the SEM. Figure 10 shows the variation of surface electric and magnetic field values in the iris (high electric field) region.

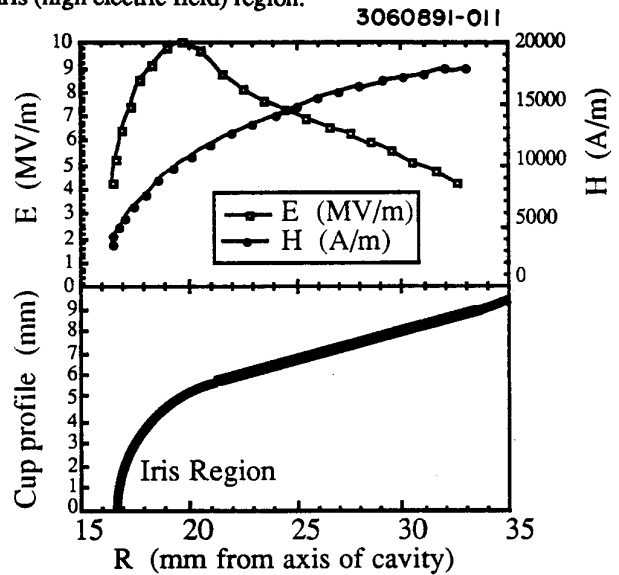


Figure 10. Surface electric and magnetic field values scaled to $E_{peak} = 10$ MV/m, along with S-band cup profile in the iris/high electric field regions. (Calculations and diagram from D. Moffat).

TABLE 1: CAVITY PREPARATIONS AND TEST CONDITIONS FOR SINGLE CELL CAVITIES EXAMINED IN SEM		
Cavity	Preparation	Test Conditions
S3C1-7	2 mins BCP (1:1:2)	low power, HPP w/ $E_{pk} \leq 72$ MV/m; temperature maps
S3C1-4	2 mins BCP (1:1:2)	low power only $E_{pk} \leq 41$ MV/m temperature maps
S3C1-2	1 hour Nitric Acid; 2 mins BCP (1:1:2)	low power, HPP w/ $E_{pk} \leq 67$ MV/m; no temperature maps

Table 1 describes the treatment and test condition of each of the cavities which have been examined in the SEM. Table 2 shows the number of "starburst" type features found in each of the cavities, as well as what foreign elements were present. "Starburst" is the term we have given the darkened regions on the niobium surface (See Figure 12). Top and bottom refer to the cavity orientation on the test stand during RF tests.

Investigation of the first cavity surface (S3C1-7) revealed 37 "starburst" features similar to those found in the mushroom cavity. Of these 37 features, 19 of them had indium present and 2 had copper, as detected by x-ray analysis in the SEM. The presence of indium can be directly attributed to the indium

TABLE 2: NUMBER OF STARBURSTS AND FOREIGN ELEMENTS FOUND IN SEM INVESTIGATIONS OF SINGLE CELL S-BAND CAVITIES		
Cavity	Number of Sites	Foreign Elements
S3C1-7	37 (23 on bottom cell, 14 on top cell)	In (51% of spots) Cu (5%)
S3C1-4	2 (2 on bottom, 0 on top)	Cu (100%)
S3C1-2	15 (14 on bottom, 1 on top)	Fe (60%) Fe&Cr (27%)

wire used for vacuum seals on the beam tubes. These seals are approximately 1.5" (3.75 cm) from the cavity irises. Indium could enter the cavity either during assembly of the gasket or during the cleaning of the cavity between tests. In order to determine when the indium contamination was occurring, another cavity (S3C1-2) was tested under similar conditions, except for the inclusion of a one hour soak of the cavity in nitric acid prior to the 2 minute etch in BCP. It was anticipated that the nitric acid soak would remove any trace of indium or copper from the cleanup or from previous tests. Upon examination of this cavity, indeed no indium or copper was found in any of the starbursts. We are therefore lead to the conclusion that the source of the indium was the process of removing the indium from the flanges. This conclusion was further supported by a simple test which showed that 2 minutes of 1:1:2 BCP has little or no effect on indium on a niobium surface. Between tests, the indium was removed with a copper scraping tool, and this process occurred every time the cavity was demounted, etched and remounted. The copper contamination could also have come from this source, however it also could come from the transmitted power probe located above the cavity.

The nitric acid soak has now been incorporated into our standard procedure prior to every test. (See Section 1 above.)

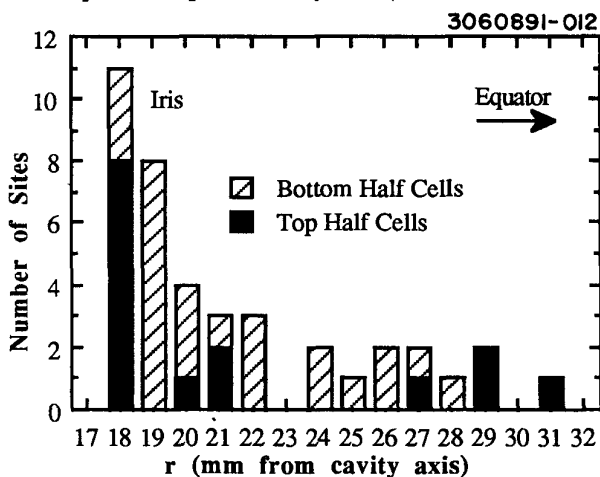


Figure 11. Radial distribution of "starburst" sites in all cavities examined to date.

Our present hypothesis is that each of these starbursts is associated with the "processing" of an emission site. Figure 8

shows a histogram of the distribution of sites in all cavities which have been examined. Comparison of Figures 10 and 11 shows that these sites are concentrated in high electric field regions. When the local electric field is strong enough, it will induce a field emission current sufficient to vaporize a small region of the RF surface, thus the starburst sites are expected to be in the high field regions of the RF surface. It is also significant that the number of starbursts in cavity S3C1-2 was only two, since the maximum peak field was only 41 MV/m. This corresponds to an emitter density of $\sim 0.1/\text{cm}^2$, considering that about 10 cm^2 of surface area is exposed to high fields in the 3 GHz cavity. If we ignore the indium contamination in cavity S3C1-7, the emitter density rises to $2/\text{cm}^2$ at $E_{\text{peak}} = 70 \text{ MV/m}$. This is in reasonable agreement with previous predictions of expected emitter density based on 1.5 GHz studies[8].

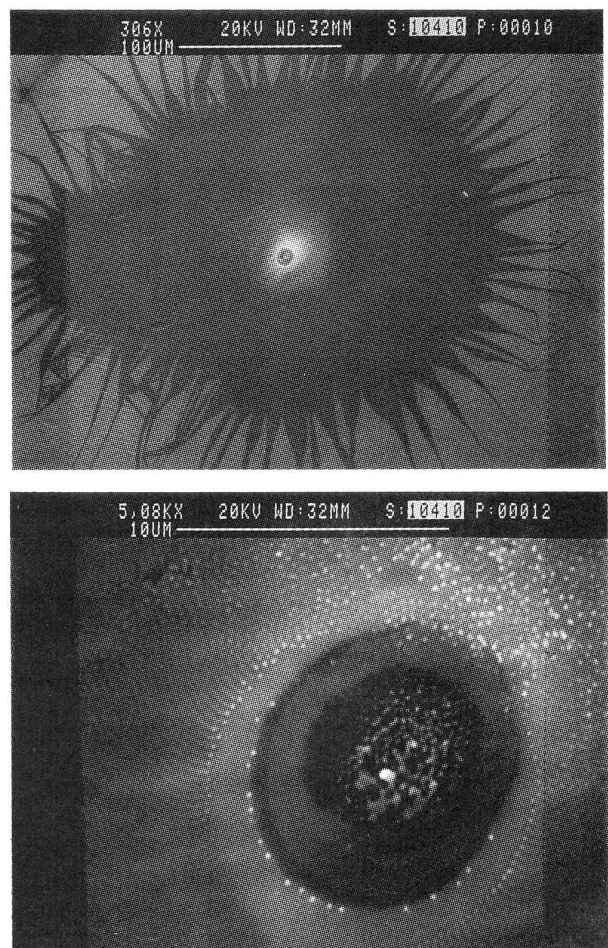


Figure 12. An example of a "starburst" phenomena found on the inside of a 3 GHz cavity in a region known, through thermometry, to have been a strong emission area. The bottom picture in an expanded view of the center of the top picture.

This investigation is being continued to further characterize the events which lead up to an explosive processing event.

Attempts are also underway to correlate surface phenomena with the temperature maps obtained during the cold tests.

The microscopic sites and the present models bear a strong similarity to DC sparking studies [9-12], as well as RF processing results in normal conducting structures[13]. A more complete discussion of our SEM investigations, both S-band and Mushroom, is being presented in an invited talk at this Workshop[14].

Application to Multi-Cell Structures

Accelerators generally use multi-cell cavities as opposed to the single cell cavities which have been investigated for basic research. As a first step, it is important to demonstrate the applicability of the HPP technique to multi-cell structures. To this end, we have fabricated (initial RRR = 250) and performed tests on a nine cell 3 GHz cavity. The results have been very successful. Figure 13a shows the Q vs. E_{peak} results for the initial test of this cavity. Prior to HPP, the cavity was limited by heavy field emission to E_{acc} = 9.5 MV/m with Q = 1.3 × 10⁹. Following HPP, the cavity reached E_{acc} = 15 MV/m with Q = 6.0 × 10⁹, a significant reduction in FE loading. The maximum field was limited by local thermal breakdown. The cavity was then sent to Wuppertal for heat treatment with Titanium to raise the RRR to 450-500.

Upon return the cavity received a two minute etch in 1:1:2 BCP and then was tested. The initial and final Q vs. E_{acc} plots are shown in Figure 13b. Processing was done with input power ≤ 80 kW, and accelerating gradient ≤ 24 MV/m. Prior to HPP, the cavity reached E_{acc} = 14 MV/m, with Q = 2 × 10⁹ with heavy field emission. Following HPP, the cavity reached E_{acc} = 20.3 MV/m, with Q = 4 × 10⁹. Field emission was still present, but, this test was halted by electrical breakdown of a vacuum window.

Following replacement of the faulty window and 2 more minutes of BCP (1:1:2), the cavity was again tested. The results of this test are shown in Figure 8c. The additional etching appears to have contaminated the RF surface with hydrogen (again see reference 3), as evidenced by the drop in low field Q value from 2 × 10¹⁰ to 5 × 10⁹. Despite this Q drop, the cavity was able to reach E_{acc} = 12 MV/m (Q = 1.3 × 10⁹) on initial rise, and E_{acc} = 19 MV/m (Q = 3 × 10⁹) following HPP processing with input power ≤ 200 kW, and E_{acc} ≤ 27 MV/m. This cavity will be re-etched and heat treated at 900° C for hydrogen removal prior to further tests.

III. CONCLUSIONS

HPP Processing has been shown to be an effective means of increasing electric fields in chemically treated single cell cavities to E_{peak} = 50-55 MV/m. Benefits increase with field level reachable during processing. The maximum processing surface field of 72 MV/m appears to be limited by a global thermal breakdown. By the same effect, the cw maximum field reachable is limited to 55 MV/m. To use this method to reach higher cw fields in single cell cavities it will be necessary to either (a) lower the frequency or (b) use a cavity with a

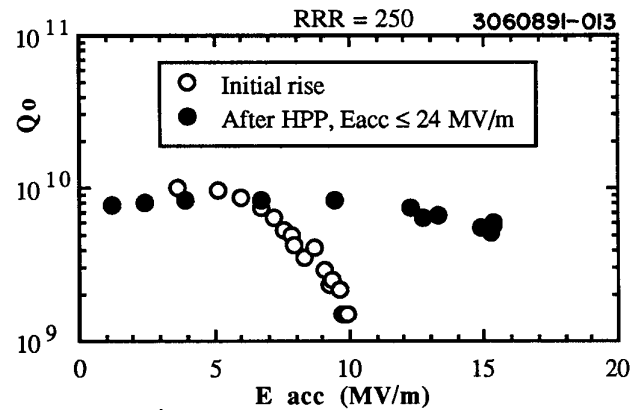


Figure 13a. Q vs E_{acc} plot for 9 cell cavity S3C9-1 before and after HPP Processing, 29-30 August 1991.

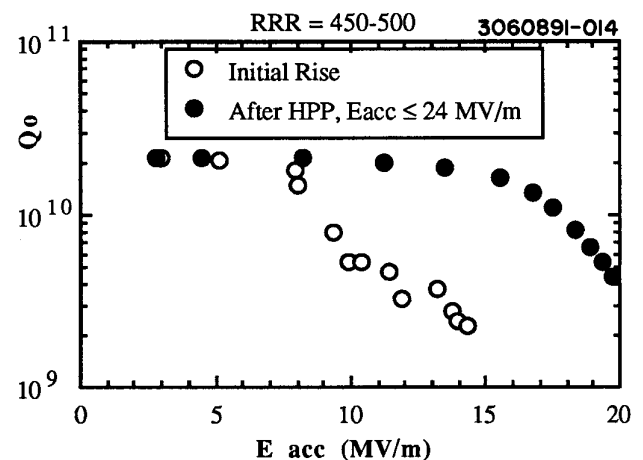


Figure 13b. Q vs E_{acc} plot for 9 cell cavity S3C9-1 before and after HPP Processing, 02-03 July 1991.

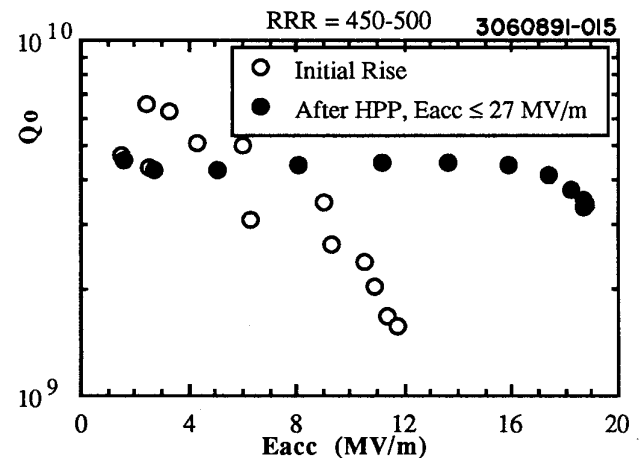


Figure 13c. Q vs E_{acc} plot for 9 cell cavity S3C9-1 before and after HPP Processing, 23 July 1991.

reduced Hpk/Epk ratio - both in order to avoid the phenomenon of GTI.

Microscopic examination of single cell cavities has shown that the number of sites processed (as indicated by a starburst feature) increased substantially over the number of sites processed using low power processing. When $E_{\text{peak}} = 40$ MV/m was reached with cw power alone, only a few emitters are processed, as revealed by the starburst features. Reaching $E_{\text{peak}} = 70$ MV/m with HPP processed several tens of emitters and allowed cw fields of up to $E_{\text{peak}} = 55$ MV/m.

HPP has been successfully used on a nine cell cavity on three separate occasions. Achievable accelerating gradients have been increased from 10-14 MV/m to 16-20 MV/m through high power pulsed processing, with significant reduction in field emission loading of the cavity.

IV. ACKNOWLEDGEMENTS

We are grateful to William Dickinson for performing much of the labor to create the temperature mapping apparatus, and to Mirang Yoon for performing calculations related to the GTI phenomenon.

Special acknowledgement goes to the SRF group at Wuppertal for the firing of the nine cell cavity. We look forward to further collaborations.

V. REFERENCES

1. J. Graber, et.al., *Proceedings of the 4th Workshop on RF Superconductivity*, KEK, Tsukuba, Japan, August 14-18, 1989, pp. 529-537.
2. J.Kirchgessner, et.al., *Proceedings of the 1989 IEEE Particle Accelerator Conference*, Chicago, DC, March 20-23, 1989, pp. 482-484.
3. J. Graber, et.al., PTP12, *Proceedings of the 1991 IEEE Particle Accelerator Conference*, San Francisco, CA, May 6-9, 1991, to be published.
4. H. Padamsee et.al., *Proceedings of the 1987 IEEE Particle Accelerator Conference*, Washington, DC, March 16-19, 1987, pp. 1824-1826.
5. D. Moffat, et.al., PTP13, *Proceedings of the 1991 IEEE Particle Accelerator Conference*, San Francisco, CA, May 6-9, 1991, to be published.
6. J. Graber, et.al., CLNS 91/1061.
7. D. Moffat, et.al., BGR2, *Proceedings of the 1991 IEEE Particle Accelerator Conference*, San Francisco, CA, May 6-9, 1991, to be published.
8. H.Padamsee, et.al., *Proceedings of the 4th Workshop on RF Super-conductivity*, KEK, Tsukuba, Japan, August 14-18, 1989, pp. 207-248.
9. B. Jüttner, *Nuclear Instruments and Methods in Physics Research*, A268 (1988), pp. 390-396.
10. M. Van Straaten, et.al., *International Journal of Mass Spectrometry and Ion Processes*, 93 (1989), pp. 125-140.
11. V.I. Rakhovsky, G.A. Mesyats, *IEEE Trans. Plas. Sci.*, PS-15, No. 5, (1987), p. 481.
12. G.A. Mesyats, *IEEE Trans. Elec. Ins.*, EI-18, No. 3, (1983), p. 218.
13. G.A. Loew and J.W. Wang, SLAC-PUB-4647 (May 1988).
14. D. Moffat, et.al., this workshop.